



Research Article

Light-induced reversible phase transition in polyvinylidene fluoride-based nanocomposites

Pamarti Viswanath¹  · Masamichi Yoshimura¹

Received: 26 August 2019 / Accepted: 22 October 2019 / Published online: 31 October 2019
© Springer Nature Switzerland AG 2019

Abstract

We report switching behavior between the ferroelectric β phase and the paraelectric α phase in polyvinylidene fluoride–multiwalled carbon nanotube (PVDF–CNT) nanocomposite. The PVDF–CNT nanocomposite thin films are prepared on Au/Si substrates using spin coating technique. Various characterization techniques reveal the interaction of PVDF with CNTs as a nucleating agent for nucleating ferroelectric β phase in PVDF. A wavelength-independent reversible phase transformation behavior is observed for the PVDF–CNT nanocomposite during the measurement of laser power modulated micro-Raman spectroscopy (533 and 632 nm lasers). This observation opens up an innovative route where we can control the interactions between polar nanocarbons and PVDF using visible light.

Keywords Phase transition · PVDF thin films · Ferroelectricity · Light driven · CNT · Raman spectroscopy

1 Introduction

The active optical control of ferroelectric properties of material has received great interest in recent years due to its varied application in ferroelectric devices such as ferroelectric memories and electro-optic modulators [1, 2]. Although spontaneous polarization of a ferroelectric material is largely controlled using an external electric field, the ferroelectric and paraelectric nature of any non-centrosymmetric material is predominantly determined by its Curie temperature [3]. The control of the polarization of a ferroelectric material determines its usage in many ferroelectric devices such as memories, field effect transistors (FETs), and electro-optic modulators, which are polarization dependent [4–6]. Mainly light interacts with a ferroelectric material thermally or electronically. For light to interact electronically with the polarization vector of the ferroelectric material, the material should possess crystal symmetry as seen generally in single-crystalline materials which are difficult to fabricate [7]. In a polycrystalline

system, the dependence of polarization of light with the spontaneous polarization vector for a ferroelectric material is ruled out due to its random domain orientations. Hence, it is very challenging to understand the effects of light–matter interactions electronically or thermally due to the random arrangement of ferroelectric domains.

Very recently, the light polarization-dependent optical control of the ferroelectric properties in single-crystalline ferroelectric thin film materials such as BaTiO_3 and BiFeO_3 has been reported for non-contact and remote manipulation of ferroelectric properties in ferroelectric-based devices [1, 8–10]. Therefore, there is an urgent need to develop new materials and strategies, which can exhibit ferroelectric nature with simultaneous control of its polarization using light. Henceforth, it remains a challenging task to switch between the ferroelectric and paraelectric phases of a non-centrosymmetric material in short timescales.

Polyvinylidene fluoride (PVDF) has received great attention as a semicrystalline polymer for its good mechanical

✉ Pamarti Viswanath, sd18603@toyota-ti.ac.jp | ¹Surface Science Laboratory, Graduate School of Engineering, Toyota Technological Institute, 2-12-1 Hisakata, Tenpaku, Nagoya 468-8511, Japan.



robustness and functionality in comparison with single-crystalline materials [11–13]. PVDF is known to exhibit ferroelectric, piezoelectric, and pyroelectric behavior, which makes it useful in many electronic devices and energy harvesting systems [14–16]. Largely, PVDF exhibits four different phases, namely α , β , γ , and δ depending on its molecular arrangement. The all *trans* (TTTT) phase (β) providing the highest spontaneous polarization exists in the orthorhombic unit cell with lattice parameters $a=8.58$ Å, $b=4.91$ Å, and $c=2.56$ Å while the *trans-gauche-trans-gauche'* (TGTG') phase (α) existing in the monoclinic unit cell configuration shows the least spontaneous polarization due to its alternate arrangement of dipoles [17, 18]. PVDF-based nanocomposites employ polar nanomaterials, which enhance its performance. Polar nanomaterials such as nanoclays, nanocarbons, and inorganic salts have been used as fillers in the PVDF matrix [19, 20]. These composites exhibit enhanced ferroelectric, dielectric, and mechanical properties which have been demonstrated for many applications [21, 22]. In this context, carbon nanotubes (CNTs) efficiently induce ferroelectric β phase in PVDF due to the electrostatic interaction of $-H^{\delta+}-C^{\delta+}-F^{\delta-}$ dipoles of PVDF with π orbitals of CNTs, as reported in the literature [23, 24].

In this work, we have observed a visible light-induced reversible phase transformation from β to α phase in PVDF–CNTs thin films probed by micro-Raman spectroscopy with two different incident laser wavelengths (532 nm, 633 nm). Various characterizations of the nanocomposites reveal the presence of stable β phase configuration under ambient conditions. We believe that this optical control of ferroelectricity in PVDF nanocomposites makes it highly desirable for various ferroelectric devices due to its mechanical robustness, simplistic preparation, and easy integration.

2 Materials and methods

PVDF–*x*CNTs ($x=0.1, 0.3, 0.5,$ and 0.7 wt%) nanocomposites were prepared by dispersing required amounts of PVDF (Alfa Aesar) in *N,N*-dimethylformamide (DMF) using a magnetic stirrer at 60 °C for 30 min and unfunctionalized CNTs (Sigma-Aldrich) in DMF (Sigma-Aldrich) by ultrasonication for 5 min. Both the PVDF solution and CNT dispersions were then mixed and ultrasonicated for 15 min to achieve a homogenous solution. The final solution was then spin-coated on Au-coated (50 nm) Si substrates to achieve a thickness of 200–300 nm by controlling the spinning rate and the viscosity of the solution. The coated substrates were then dried at 60 °C on a hot plate for an hour before using for other characterizations. Crystalline structure was revealed by micro-Raman

spectroscopy (Renishaw-InVia Raman Spectroscopy). 532-nm diode laser (green) and 632-nm He–Ne laser (red) were used to perform wavelength and laser power-dependent Raman spectroscopy. It is noted that Raman spectra were acquired at more than 5 points at different areas of the thin film (objective lens is $100\times$). Elemental composition study was performed by X-ray photoelectron spectroscopy (XPS, ULVAC-PHI PHI5000 Versa Probe II) with a source of AlK α 1486.6 eV. Differential scanning calorimetry (DSC) was done under an airflow at a heating rate of 10 °C/min, using Al crucibles (Shimadzu-TA-60WS/DTG-60H). Fourier transformation infrared spectroscopy (FTIR, Jasco, FTIR-6200) was acquired over the wave number range of 600 – 1000 cm^{-1} using attenuated total reflectance technique (ATR) for thin films coated on Au/Si substrates.

3 Results and discussion

Since each crystalline phase in PVDF has a unique absorbance in the infrared regime, the formation of β -phase in PVDF–CNTs thin films was confirmed by FTIR as shown in Fig. 1a. The increase in absorbance intensity of the band at 840 cm^{-1} (CH_2 rocking, CF_2 stretching, and skeletal C–C stretching corresponding to β PVDF) w.r.t the absorbance band at 796 cm^{-1} (corresponding to α phase) is seen which is due to the formation β -phase in PVDF [25–28]. Figure 1b shows the variation of the β phase of PVDF with a change in concentration of CNTs. The relative portion of β -phase in samples F(β) was quantified from IR spectra using Beer–Lambert law using Eq. (1) which is given as:

$$F(\beta) = \frac{A_{\beta}}{\frac{K_{\beta}}{K_{\alpha}}(A_{\alpha} + A_{\beta})} \quad (1)$$

where A_{α} and A_{β} are the absorbances at 764 cm^{-1} and 840 cm^{-1} , correspondingly, and K_{β} (7.7×10^4 cm^2 mol^{-1}) and K_{α} (6.1×10^4 cm^2 mol^{-1}) are the absorption coefficients at the individual wavenumber [25]. As seen from the figure, the β phase fraction increased with an increase in the CNTs content and exhibited a maximum value of 78% at 0.7 wt%. Hence, PVDF–0.7 wt% CNT composition was chosen for further studies and will be referred to as PVDF–CNTs. Figure 2 shows Raman spectra of pristine PVDF and PVDF–CNT nanocomposite. The peaks at 610 and 795 cm^{-1} correspond to the α phase, and peaks at 840 and 510 cm^{-1} correspond to the β phase.

Figure 3 shows XPS spectra (C1s and F1s) of pristine PVDF and PVDF–CNTs. Figure 3a, b shows the F1s level spectra, which are originated from F atoms in PVDF. Figure 3c, d shows C1s spectra that come from C atoms in both PVDF and CNTs. The deconvoluted spectra for the

Fig. 1 **a** FTIR spectra of pristine PVDF–CNTs thin films of different loadings and **b** β phase fraction in PVDF–CNTs for different CNT loadings

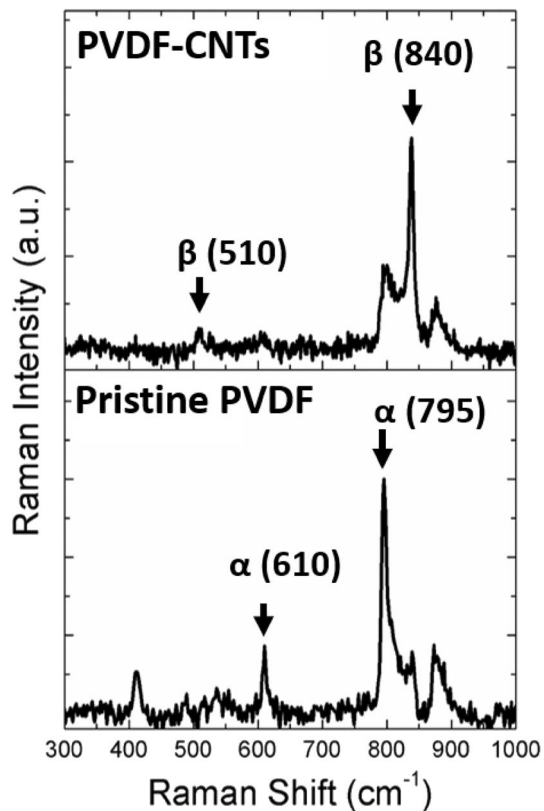
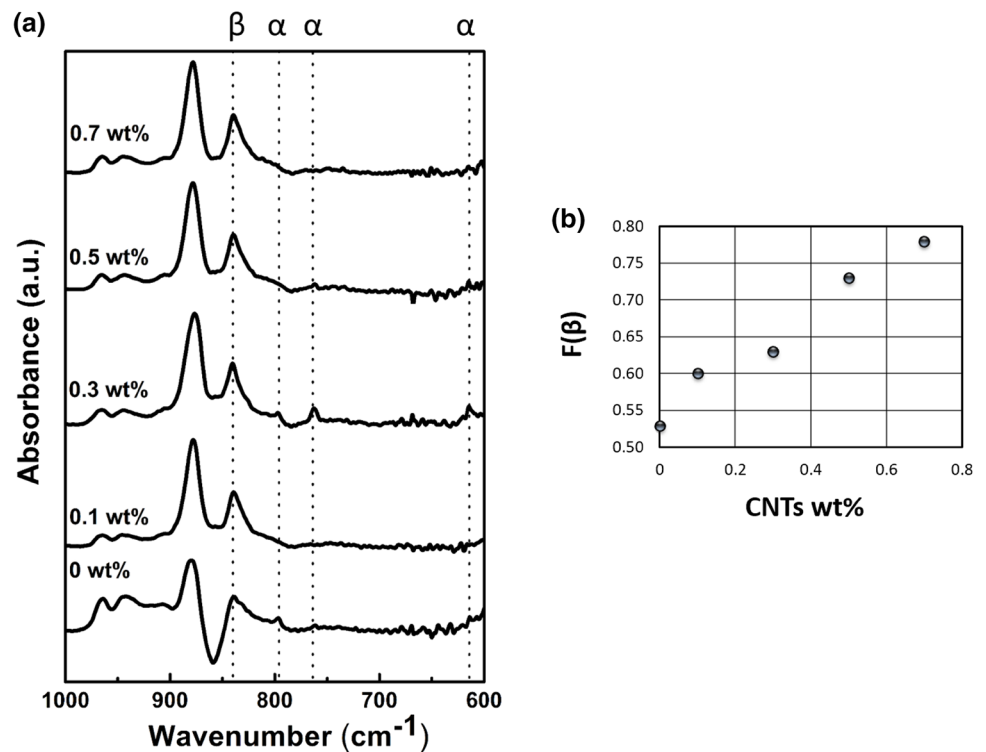


Fig. 2 Raman spectra of pristine PVDF and PVDF–CNT nanocomposite

C1s also show the contribution of various C species to the C1s XPS spectra. Two major peaks from contributions of $-\text{CH}_2-$ and $-\text{CF}_2-$ species are seen in the C1s spectra of pristine PVDF and PVDF–CNT nanocomposite. A less intense peak at 292.9 eV in C1s spectra of pristine PVDF indicates the presence of $-\text{CF}_3-$ species. In the case of PVDF–CNTs, contributions of $-\text{CH}_2-$ and $-\text{CF}_2-$ species are observed at 286.5 eV and 290.9 eV, which are 0.7 eV and 0.5 eV higher than those of pure PVDF, which indicates a shift of the C1s spectra of PVDF–CNT nanocomposite toward higher binding energy. The peak at 284.5 eV in the C1s spectra of PVDF–CNTs indicates the sp^2 contributions of C atoms in CNTs. In addition, there is a decrease in peak area corresponding to CF_2 and broadening of overall C1s spectra as compared to C1s spectra of pristine PVDF. Two new peaks at 288.8 eV and 281.4 eV in PVDF–CNTs appeared which are assigned to $-\text{F}-\text{C}-\text{H}-$ and $-\text{F}-\text{C}-\text{C}-\text{H}-$ (crosslinking of polymer chains) species of PVDF [29]. The shift of the C1s spectra can be due to the change in the electronic environment of C species in PVDF in the presence of CNTs. The chemical shift in C1s spectra of PVDF in the presence of nanostructures with electrostatic charges on the surface is reported in the literature [30–32]. Overall, the chemical shift, peak broadening, and appearance of new peaks indicate a strong electrostatic interaction of PVDF molecules to CNT's with a simultaneous ordering of PVDF molecules in the form of β -phase. The XPS spectra of F1s for the pure PVDF showed a peak located at 688.5 eV corresponding to F atoms in $-\text{CF}_2-$ species. For the nanocomposite, it was

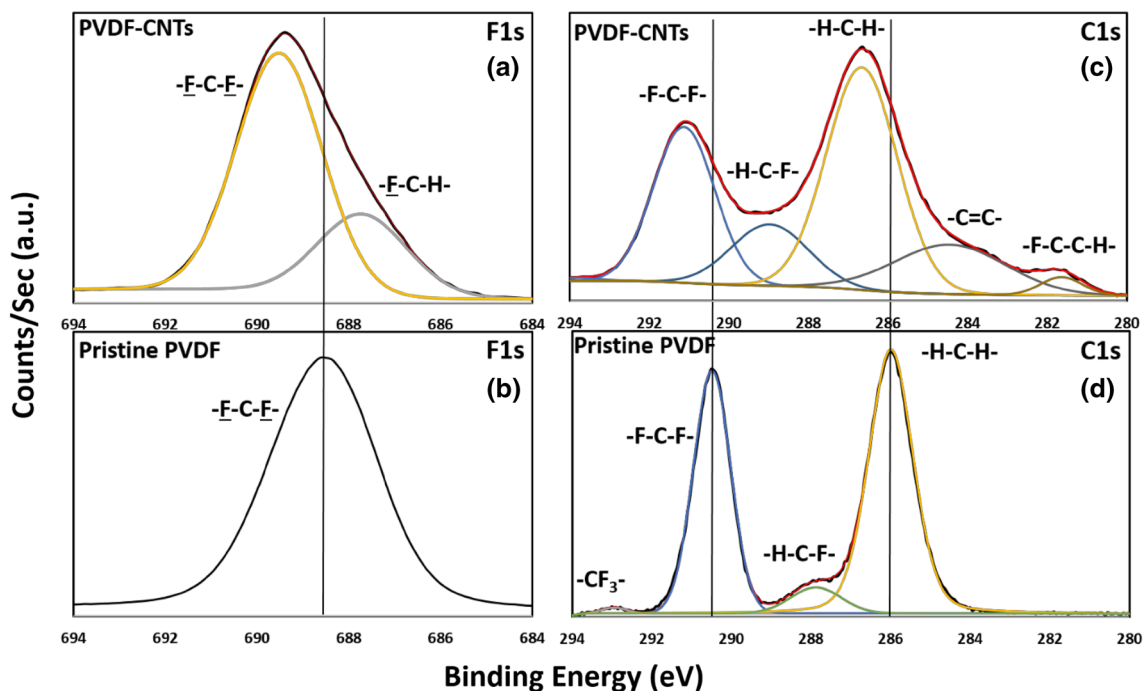


Fig. 3 XPS measurements for PVDF–CNTs and pristine PVDF. F1s core level spectra of **a** PVDF–CNTs, **b** pristine PVDF. C1s core level spectra of **c** PVDF–CNTs and **d** pristine PVDF

located at 689.4 eV along with the appearance of the new peak at 687.6 eV upon deconvolution [33]. The new peak at 687.6 corresponds to F atom in –H–C–F– species. Also, XPS peaks of F1s for PVDF–CNT nanocomposite shift to higher binding energies, due to the chemical shift induced by the surface interfacial interactions between the hydrogen atoms in –H^{δ+}–C^{δ+}–F^{δ-}– dipoles of PVDF and the π orbitals of CNTs.

The phase transformation phenomena were investigated using laser power-dependent micro-Raman spectroscopy (533- and 632-nm incident lasers using a 100× objective lens with a laser spot area of 0.5–1 μm²) to observe the structural changes. Figure 4 shows the Raman spectra with increasing laser powers (λ=532 nm) for PVDF–CNTs where the phase transformation behavior was seen. At laser powers less than 2.4 mW, peaks at 840 and 510 cm⁻¹ indicate that the β phase is predominantly present. While above 1.4 mW, such peaks shrank and two peaks at 610 and 795 cm⁻¹ corresponding to the α phase appear [34, 35]. At higher laser powers (beyond 2.4 mW), the thin film thermally degraded. When the laser power was reduced below 1.4 mW (threshold power), the α phase transformed into the β phase in a reversible fashion. Further, we found that this reversible phenomenon is not wavelength dependent by acquiring the Raman spectra at two different wavelengths 533 nm and 632 nm.

To see whether the phase transformation behavior is switchable, we captured that the Raman spectra

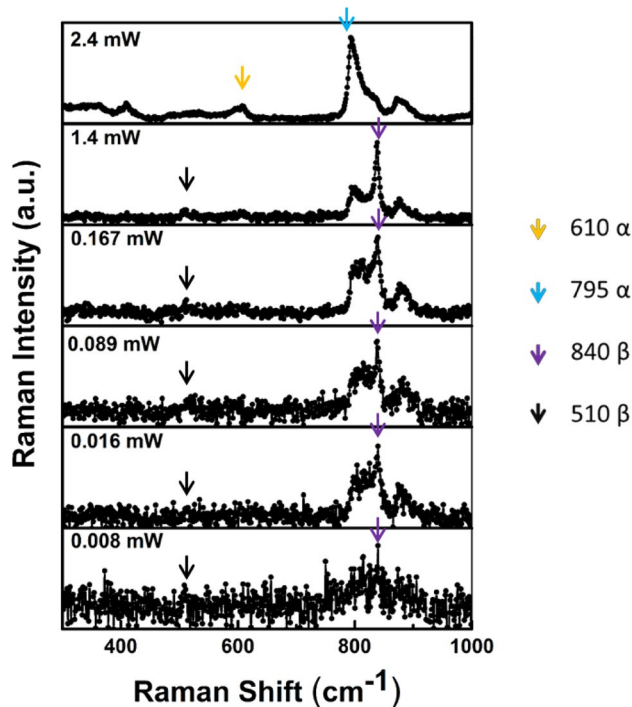


Fig. 4 Raman spectra with increasing laser powers for PVDF–CNTs showing the transformation of the ferroelectric phase to the paraelectric phase (a–f) at laser powers beyond 1.4 mW (λ=532 nm)

($\lambda = 633$ nm) were obtained at low and high powers (1.4 and 2.4 mW) alternately at the same location one after other as shown in Fig. 5a. The switching behavior between the paraelectric (α phase) and ferroelectric phases (β phase) in PVDF–CNT nanocomposites is clearly seen. The intensity ratio of β over α at the laser powers of 1.4 and 2.4 mW is plotted in Fig. 5b. Regular oscillation behavior was observed, and intensity ratio changes three times approximately during the change in laser power. It is noted that for pristine PVDF, no such phase transformations were observed as shown in Fig. 6. Similar in situ laser power-dependent Raman spectroscopy was performed for other compositions of CNTs, i.e., 0.1 wt%, 0.3 wt%, and 0.5 wt% as shown in Fig. 7a. Similar switching behavior was observed for loadings of 0.3 and 0.5 wt%, whereas no phase change behavior was observed in 0.1 wt% composition. The variation of β : α intensity w.r.t laser powers for 0.3, 0.5, and 0.7 wt% is shown in Fig. 7b.

Figure 8 shows DSC heating and cooling curves for pristine PVDF and PVDF–CNT nanocomposite. The shift of crystallization temperature (T_{cr}) toward higher temperature and lowering of crystallization temperature (T_m) for the nanocomposite from the pristine condition clearly indicates the nucleation and structural modification of PVDF molecules in the presence of CNTs. Determination of Curie temperature of the ferroelectric to paraelectric transition using DSC is difficult for PVDF and its composites because the phase transition temperature and the melting temperature lie very close to each other (167–172 °C) [36]. Irrespective of this difficulty, it is very clear that the Curie temperature of PVDF is independent of the other external factors such as the addition of other nanomaterials in the PVDF matrix. Since no phase transition was observed in pristine PVDF with

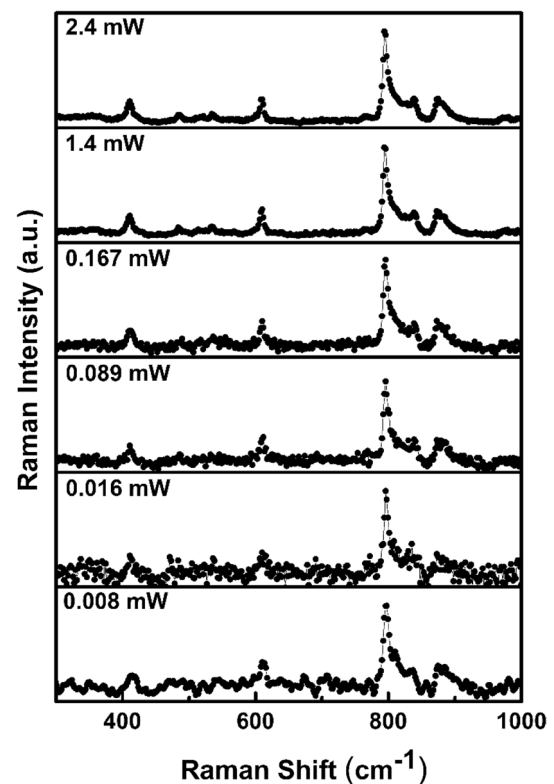
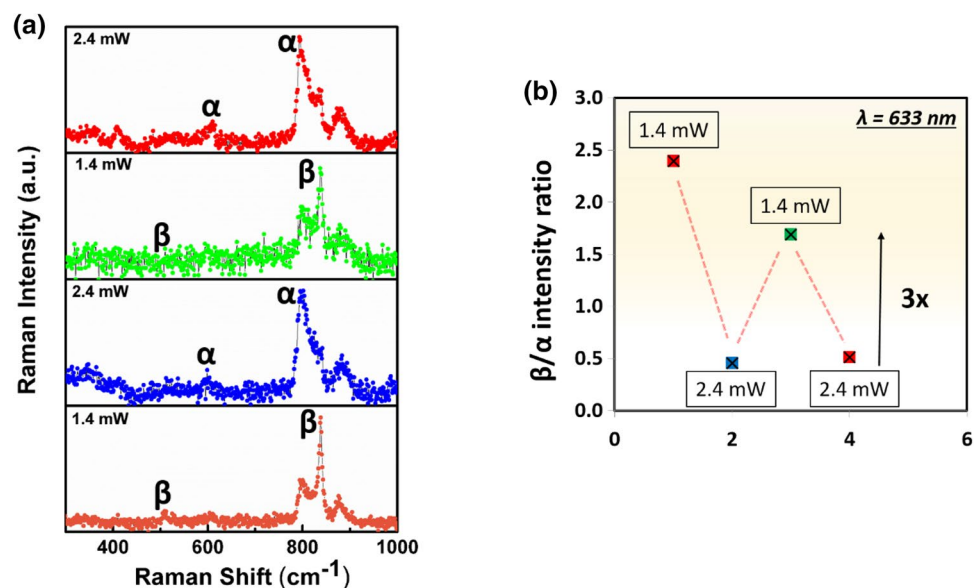


Fig. 6 Raman spectra of pristine PVDF at increasing laser powers ($\lambda = 532$ nm)

slight β phase (Fig. 6), we conclude that the increase in laser power does not produce temperatures close to the phase transition or melting in PVDF. On the other hand, laser heating with localized temperatures below the melting point cannot be ignored since the excitation is done using a continuous wave laser (without thermal

Fig. 5 Reversible switching behavior of the ferroelectric and the paraelectric phases in PVDF–CNTs w.r.t laser power change in an ON–OFF fashion from 1.4 to 2.4 mW at $\lambda = 633$ nm. **a** Raman spectra of PVDF–CNTs at laser powers of 1.4 and 2.4 mW (high/low) at the same spot under investigation. **b** β and α peak intensity ratio versus laser power high/low (β and α correspond to peak intensity ratio of 840 and 795 cm^{-1})



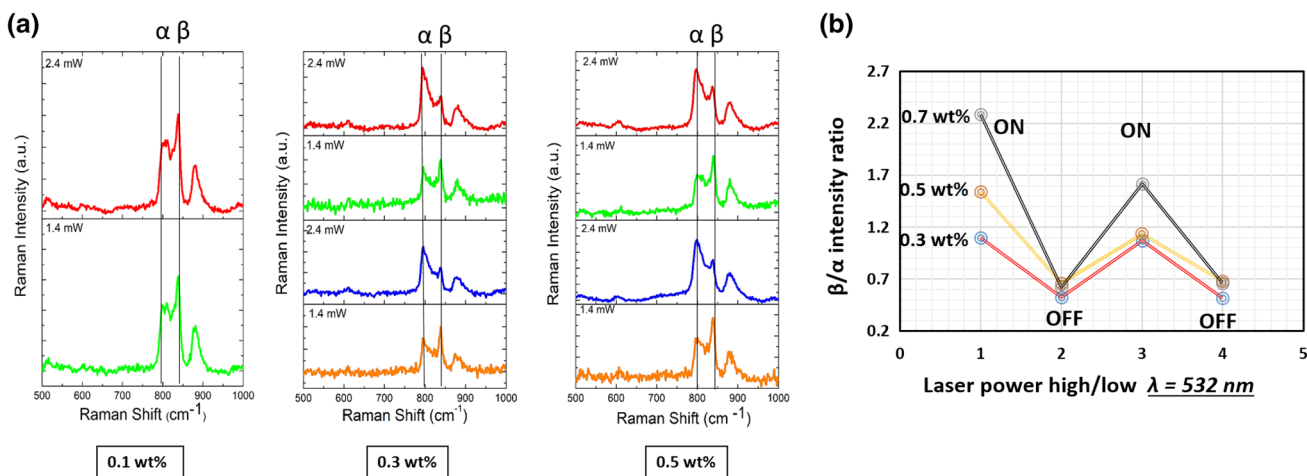
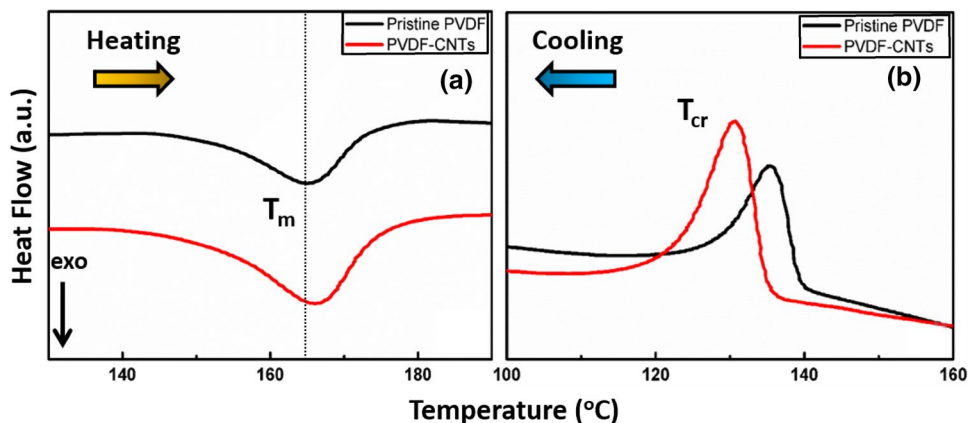


Fig. 7 Reversible phase switching behavior from 1.4 to 2.4 mW at $\lambda=532 \text{ nm}$ for different CNT loadings. **a** Raman spectra of PVDF–CNTs at laser powers of 1.4 and 2.4 mW (high/low) at the same

spot under investigation. **b** β and α peak intensity ratio versus laser power high/low (β and α correspond to the peak intensity ratio of 840 and 795 cm^{-1})

Fig. 8 DSC **a** heating and **b** cooling curves for PVDF–CNTs and Pristine PVDF

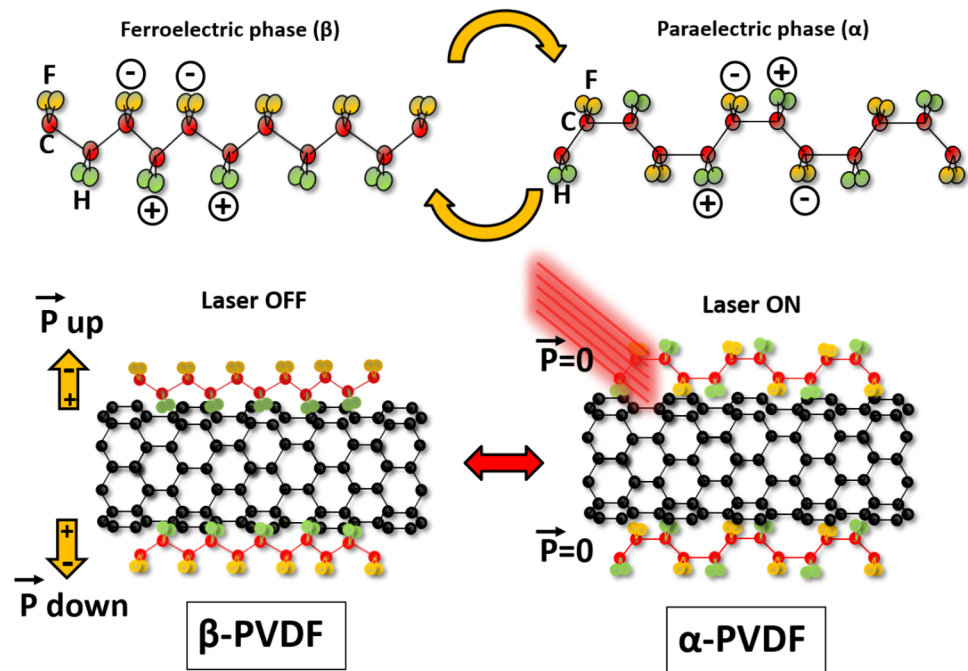


degradation of the material). The results from XPS and DSC confirm that the phase transformation occurs on the surface of CNTs where β -PVDF chains are adsorbed. Schematics of the phase transformation in PVDF chains on the surface of CNTs are shown in Fig. 9. As indicated, hydrogen atoms in PVDF possess a partial positive charge due to the presence of highly electronegative fluorine atoms in vicinity [37]. This helps the hydrogen atoms to get attached to the CNT walls due to the strong electrostatic interaction with the π orbitals of CNTs [23]. Although it is reported that the (TGTG') is energetically more stable than β (TTTT) conformation of PVDF, we still observed the phase transformation to be reversible [38]. Such an occurrence can only be attributed to the presence of CNTs in the system. Since similar results were not observed in pristine PVDF (Fig. 6), we assume that the electrostatic interaction between CNT and the polymer chains is regained at low laser powers. Thus, the laser

excitation during Raman measurements induces some temporary structural modification to the polymer chains in the presence of CNTs.

The alteration of the ferroelectric phase to the paraelectric phase can be due to several reasons. One of the reasons can be structural modification due to a localized increase in temperature by laser power. Since we employ a continuous laser source in Raman measurements, it is likely that there is some amount of heat that is generated within the material. Further, it can be expected that the localized photocurrents and pyroelectric currents generated due to laser heating combined with a decrease in electrical resistivity caused by the presence of CNTs [39–41]. The high content of β phase (non-centrosymmetric phase) in the PVDF–CNTs composite produces pyroelectricity induced charges due to a temporary voltage generated at the instant when it is excited with due to the temperature induced by the laser locally [42, 43].

Fig. 9 Schematics showing the transformation of paraelectric α from ferroelectric β phase during laser excitation near the surface of the CNTs (\vec{P} is the polarization vector)



These charges combined with the photocurrents induced with the laser may orient the PVDF molecules adsorbed on the surface of the CNTs to its energetically stable α (TGTG') conformation during the laser excitation (Fig. 9). Hence, CNTs act no longer as β nucleation sites during laser excitation with high powers. This suggests that the phase change occurs at the interface of PVDF chains and the CNT surface. In the case where the CNT loading was 0.1 wt%, no transformation behavior was observed. This can be because of the low electrical conductivity of the composite at low CNT loadings, whereas for loadings at 0.3, 0.5, and 0.7 wt%, the phase transformation behavior was observed. It is also known that the conductivity increases beyond the percolation threshold of the material, which is reflected in the decrease in dielectric constant and increase in dielectric loss. In the case of CNTs, the conductivity increases rapidly after 0.4 wt% loading in PVDF in general [39]. This may also suggest that the change in local conductivity can also affect the phase transformation behavior. It is also noted that the decrease in CNTs content induces lower β fraction and hence lower pyroelectric current [17, 44]. Therefore, the absence of phase transformation behavior in lower CNT loading can be due to the lower pyroelectric currents with less electrical conductivity. The reversible phase change implies variations in the crystal structure of β -phase to α phase and, thereby, the dimensions of the material exhibiting photostrictive nature. The β phase has an orthorhombic structure, which exhibits different crystal dimensions and spontaneous polarization when compared with the paraelectric α phase. Hence, the demonstrated dynamic reversible optical control of the

ferroelectric polarization in very small areas will be a key vital in ferroelectric devices and materials.

4 Conclusions

We report a light-driven wavelength-independent ferroelectric β phase to paraelectric α phase reversible transition in PVDF–CNTs composite thin films. CNTs act as the nucleating site for the formation of β phase as confirmed by the structural characterizations. Laser power-dependent Raman spectroscopy shows the reversible phase transition phenomenon, which is expected to arise due to the generation of laser-induced pyroelectric currents. From the supporting results from XPS and DSC, we confirm that the phase transformation process occurs on the surface of CNTs where β -PVDF chains are adsorbed. The reversible recovery of the ferroelectric β phase from the paraelectric α phase using visible light suggests that formation of the nanocomposites with nanocarbons can modify the ferroelectric properties of crystalline polymer materials. These findings will be helpful in ferroelectric memory-based devices and other related applications.

Acknowledgements This study is supported in part by Strategic Research Foundation Grant-aided Project for Private Universities from MEXT.

Compliance with ethical standards

Conflict of interest On behalf of all authors, the corresponding author states that there is no conflict of interest.

References

- Rubio-Marcos F et al (2018) Reversible optical control of macroscopic polarization in ferroelectrics. *Nat Photonics* 12:29–32
- Nalwa HS (1995) *Ferroelectric polymers: chemistry, physics, and applications*. CRC Press, Boca Raton
- Eric Cross L (1987) Relaxor ferroelectrics. *Ferroelectrics* 76:241–267
- Hwang SK, Bae I, Kim RH, Park C (2012) Flexible non-volatile ferroelectric polymer memory with gate-controlled multilevel operation. *Adv Mater* 24:5910–5914
- Silibin MV et al (2017) Applied surface science local mechanical and electromechanical properties of the P (VDF-TrFE)-graphene oxide thin films. *Appl Surf Sci* 421:42–51
- Chiappone A et al (2018) In situ generation of silver nanoparticles in PVDF for the development of resistive switching devices. *Appl Surf Sci* 455:418–424
- Yang MM, Alexe M (2018) Light-induced reversible control of ferroelectric polarization in BiFeO₃. *Adv Mater* 30:1–6
- Rubio-Marcos F, Campo A Del, Marchet P, Fernández JF (2015) Ferroelectric domain wall motion induced by polarized light. *Nat Commun* 6:6594
- Páez-Margarit D et al (2018) Light-induced capacitance tunability in ferroelectric crystals. *ACS Appl Mater Interfaces* 10:21804–21807
- Li T et al (2018) Optical control of polarization in ferroelectric heterostructures. *Nat Commun* 9:3344
- Fan FR, Tang W, Wang ZL (2016) Flexible nanogenerators for energy harvesting and self-powered electronics. *Adv Mater* 28:4283–4305
- Zhang W et al (2013) Superhydrophobic and superoleophilic PVDF membranes for effective separation of water-in-oil emulsions with high flux. *Adv Mater Lett* 25:2071–2076
- Wang S et al (2015) In-situ combined dual-layer CNT/PVDF membrane for electrically-enhanced fouling resistance. *J Membr Sci* 491:37–44
- Lee JP, Lee JW, Baik JM (2018) The progress of PVDF as a functional material for triboelectric nanogenerators and self-powered sensors. *Micromachines* 9:532
- Shi K, Sun B, Huang X, Jiang P (2018) Synergistic effect of graphene nanosheet and BaTiO₃ nanoparticles on performance enhancement of electropun PVDF nanofiber mat for flexible piezoelectric nanogenerators. *Nano Energy* 52:153–162
- Caparros C, Lopes AC, Ferdov S, Lanceros-Mendez S (2013) γ -Phase nucleation and electrical response of poly(vinylidene fluoride)/microporous titanosilicates composites. *Mater Chem Phys* 138:553–558
- Martins P, Lopes AC, Lanceros-Mendez S (2014) Electroactive phases of poly(vinylidene fluoride): determination, processing and applications. *Prog Polym Sci* 39:683–706
- Ruan L et al (2018) Properties and applications of the β phase poly(vinylidene fluoride). *Polymers (Basel)* 10:1–27
- Ma Y, Luo H, Guo R, Zhou K, Zhang D (2018) Enhanced performance in multilayer-structured nanocomposites using BaTiO₃ and Ba_{0.8}Sr_{0.2}TiO₃ decorated graphene hybrids. *Ceram Int* 44:20871–20876
- Bodkhe S, Rajesh PSM, Kamle S (2014) Beta-phase enhancement in polyvinylidene fluoride through filler addition: comparing cellulose with carbon nanotubes and clay. *J Polym Res* 21:434
- Tian BB et al (2016) Tunnel electroresistance through organic ferroelectrics. *Nat Commun* 7:1–6
- Cheon S, Kang H, Kim H, Son Y, Lee JY, Shin H-J, Kim S-W, Cho JH (2017) *Adv. Funct. Mater.* 28:1703778
- Yu S et al (2009) Formation mechanism of β -phase in PVDF/CNT composite prepared by the sonication method. *Macromolecules* 42:8870–8874
- Kim GH, Hong M, Seo Y (2009) Piezoelectric properties of poly(vinylidene fluoride) and carbon nanotube blends: β -phase development. *Phys Chem Chem Phys* 11:10506–10512
- Salimi A, Yousefi AA (2003) FTIR studies of β -phase crystal formation in stretched PVDF films. *Polym Test* 22:699–704
- Asai K, Okamoto M, Tashiro K (2008) Crystallization behavior of nano-composite based on poly(vinylidene fluoride) and organically modified layered titanate. *Polymer (Guildf)* 49:4298–4306
- Nallasamy P, Mohan S (2005) Vibrational spectroscopic characterization of form II poly(vinylidene fluoride). *Indian J Pure Appl Phys* 43:821–827
- Wu X et al (2016) Synthesis and adsorption properties of halloysite/carbon nanocomposites and halloysite-derived carbon nanotubes. *Appl Clay Sci* 119:284–293
- Zhang W et al (2013) Superhydrophobic and superoleophilic PVDF membranes for effective separation of water-in-oil emulsions with high flux. *Adv Mater* 25:2071–2076
- Biswas A, Garain S, Maity K, Henkel K, Schmeißer D, Mandal D (2019) Influence of in situ synthesized bismuth oxide nanostructures in self-poled PVDF-based nanogenerator for mechanical energy harvesting application. *Polym Compos* 40:E265–E274
- Tamang A, Ghosh SK, Garain S, Alam M, Haeberle J (2015) DNA-assisted β -phase nucleation and alignment of molecular dipoles in PVDF film: a realization of self-poled bioinspired flexible polymer nanogenerator for portable electronic devices. *ACS Appl Mater Interfaces* 7:16143–16147
- Abdalla S, Obaid A, Al-marzouki FM (2016) Preparation and characterization of poly(vinylidene fluoride): a high dielectric performance nano-composite for electrical storage. *Results Phys* 6:1–11
- Chakradhar RPS, Prasad G, Bera P, Anandan C (2014) Stable superhydrophobic coatings using PVDF-MWCNT nanocomposite. *Appl Surf Sci* 301:208–215
- Boccaccio T, Bottino A, Capannelli G, Piaggio P (2002) Characterization of PVDF membranes by vibrational spectroscopy. *J Membr Sci* 210:315–329
- Giacometti JA, Zucolotto V, Oliveira ON, Gozzi G, Chinaglia DL (2005) Phase transition in poly(vinylidene fluoride) investigated with micro-Raman spectroscopy. *Appl Spectrosc* 59:275–279
- Gregorio R (2005) Determination of the α , β and γ crystalline phases of poly(vinylidene fluoride) films prepared at different conditions. *J Appl Polym Sci* 100:12–14
- Kim Sejung, Song Youngjun, Heller Michael J (2017) Influence of MWCNTs on β -Phase PVDF and triboelectric properties. *J Nanomat* 2017:7
- Bohlén M, Bolton K (2014) Conformational studies of poly(vinylidene fluoride), poly(trifluoroethylene) and poly(vinylidene fluoride-co-trifluoroethylene) using density functional theory. *Phys Chem Chem Phys* 16:12929–12939
- Barrau S et al (2018) Nanoscale investigations of α - and γ -crystal phases in PVDF-based nanocomposites. *ACS Appl Mater Interfaces* 10:13092–13099
- Zhao H, Yang M-H, He D, Bai J (2016) Enhanced dielectric performance of polyvinylidene fluoride composites with an all-carbon hybrid architecture: vertically aligned carbon nanotube arrays on graphite nanoplatelets. *J Mater Chem C* 4:8911–8919
- Yang M et al (2018) Largely enhanced dielectric constant of PVDF nanocomposites through a core-shell strategy. *Phys Chem Chem Phys* 20:2777–2786
- Martins P, Lopes AC, Lanceros-Mendez S (2014) Electroactive phases of poly(vinylidene fluoride): Determination, processing and applications. *Prog Polym Sci* 39(4):683–706

43. Guggilla P, Edwards M (2016) Dielectric, conductance and pyroelectric characterization of MWCNT: PVDF nanocomposite thin films for multiple device applications. *Int J Compos Mater* 6:145–151
44. Broadhurst MG, Davis GT, Mckinney JE, Collins RE (2008) Piezoelectricity and pyroelectricity in polyvinylidene fluoride—a model. *J Appl Phys* 49:4992

Publisher's Note Springer Nature remains neutral with regard to jurisdictional claims in published maps and institutional affiliations.